Green Chemistry

Controlled hydrogenation of a biomass-derived platform chemical formed by aldol-condensation of 5-hydroxymethyl furfural (HMF) and acetone over Ru, Pd, and Cu catalysts

Journal:	*Green Chemistry*
Manuscript ID	GC-ART-12-2021-004650.R1
Article Type:	Paper
Date Submitted by the Author:	08-Feb-2022
Complete List of Authors:	Gilcher, Elise; University of Wisconsin-Madison, Chemical and Biological Engineering Chang, Hochan; University of Wisconsin Madison, Chemical and Biological Engineering Huber, George; University of Wisconsin, Chemical and Biological Engineering Dumesic, James; University of Wisconsin Madison, Chemical and Biological Engineering

ARTICLE

Controlled hydrogenation of a biomass-derived platform chemical formed by aldol-condensation of 5-hydroxymethyl furfural (HMF) and acetone over Ru, Pd, and Cu catalysts

Received 00th January 20xx,
Accepted 00th January 20xx

DOI: 10.1039/x0xx00000x

Elise B. Gilcher, [a,b] Hochan Chang, [a] George W. Huber [a] and James A. Dumesic[a,b]*

We studied the hydrogenation at temperatures from 313 – 393 K of a biomass-derived platform molecule, 5-hydroxymethyl furfural (HMF)-Acetone-HMF (HAH) over Pd, Ru, and Cu based catalysts. HAH was selectively hydrogenated to produce partially-hydrogenated monomers (PHAH) over Cu and Ru catalysts and to fully-hydrogenated HAH monomers (FHAH) over the Ru catalyst. Pd based catalysts yielded a mixture of partially and fully hydrogenated monomers. Lumped reaction kinetics models were employed to quantify the kinetic behavior for hydrogenation over Ru, Cu, and Pd catalysts. The 5-step pathway exhibited over Pd and Ru catalysts consists of both series and parallel reaction steps, where HAH is both converted to fully hydrogenated products sequentially via series reactions of partially hydrogenated intermediates, as well as converted directly in parallel reactions to form the fully hydrogenated products. In contrast, the 3-step pathway over the Cu catalyst consists only of the consecutive reaction steps, where the final product was formed via series reactions of intermediate products. Additionally, reaction over the Cu catalyst did not hydrogenate the furan rings of the HAH molecule and yielded a different final product than those hydrogenation over Pd and Ru catalysts. Batch conditions are determined for each hydrogenated product that give the highest yields in both batch and plug flow reactors.

Introduction

Concerns of increasing CO_2 emissions and dependency on petroleum-based products have renewed interest in synthesizing renewable fuels, polymeric materials, and high value commodity chemicals from biomass-derived sources. 5-Hydromethylfurfural (HMF) is a versatile, biomass-derived platform molecule that can be sustainably synthesized by the selective dehydration of glucose, fructose, and polysaccharides in high yields at laboratory scale.[1-3] HMF has been explored as a precursor to various high value chemicals and chemical precursors, such as 2,5-furandicarboxilic acid (FDCA)[4-6], dimethyl furan (DMF)[7-10], and di-hydroxy-methyl-tetrahydrofuran (DHMTHF)[11,12]. Hydrogenation reactions of HMF[7,11,13,14] and similar compounds like furfural[9,15] and furan[16] have been studied in detail over various heterogeneous catalysts. For example, Alamillo et al. reported the hydrogenation of HMF over Pd, Ru, and Pt catalysts in biphasic systems, and achieved high selectivities to DHMTHF, the fully hydrogenated product, of 88 – 91 % over Ru catalysts.[11] Another study reported an 81% selectivity to DMF over Ru/C using 2-propanol as a solvent and hydrogen donor at 463 K.[7] Hydrogenation of furfural over a Cu/Fe_2O_3 catalyst in 2-propanol resulted in high selectivities of furfuryl alcohol (78%) at low conversions, while hydrogenation of furfural over Pd/Fe_2O_3 yielded further hydrogenolysis and ring opening products.[9] However, key challenges, such as trace impurities in HMF reducing further reaction yields[17] and degradation during storage (especially for HMF oils[18]), have limited the scale-up and utilization of HMF as a renewable replacement for fossil fuels[19].

The production of chemical adducts with larger molecular weights is of importance, because higher molecular weight chemicals can possess a variety of functionalities for diverse applications through robust catalytic reactions, and they potentially offer increased molecular stability of HMF-derived products. Hydrogenation studies on larger adducts with similar functionalities to HMF, typically synthesized by aldol condensation of furfural or HMF with acetone, can produce higher molecular weight molecules suitable for potential diesel and jet fuels.[20-26] For example, furfural and acetone were reacted in THF for a one-pot synthesis of base-catalyzed aldol condensation to highly conjugated compounds. The product mixture was then hydrogenated over Ru, yielding a wide distribution of fully hydrogenated products (mostly C_{13} oligomers) for potential liquid alkane applications.[27] The selective synthesis of various C_8-C_{16} linear alkanes in isolated yields of 65-87% was reported by Sutton et al. from the hydrogenation of HMF or methylfurfural condensation products over a Pd/C catalyst with acetic acid, H_2, and an inorganic La-based catalyst.[28] Other studies examined the hydrogenation of a furfural-acetone (FA, the condensate product of furfural and acetone, C_8) over alumina-supported Ru, Rh, Pd, and Pt metals. A mechanism, consisting of series, parallel, and reversible steps, and corresponding kinetic models were fit to the data. Ru and

[a] Department of Chemical and Biological Engineering, University of Wisconsin-Madison, Madison, WI, USA.
[b] DOE Great Lakes Bioenergy Research Center, University of Wisconsin-Madison, Madison, WI, USA.

† Electronic Supplementary Information (ESI) available. See DOI: 10.1039/x0xx00000x

Rh were found to hydrogenate only aliphatic double bonds, while Pd and Pt exhibited higher activity and catalyzed hydrodeoxygenation and ring opening reactions.[23] Room temperature hydrogenation was achieved for FA and furan-acetone-furan (FAF) aldol condensation adducts over a bimetallic NiPd catalyst with 99% selectivity to the fully hydrogenated products in water.[16] However, an analysis of the reaction kinetics toward high selectivity of partially hydrogenated products was not examined in these works.

Recently, our group reported the synthesis of high purity (>99 %) HMF-acetone-HMF (HAH) through base-catalyzed aldol condensation reactions.[29] HAH is a highly functionalized, platform chemical that opens pathways for the production of a wide range of C_{15} polymers[30], organic dyes, and high molecular weight liquid fuels.[29] Moreover, the synthesized HAH is a crystalline material which can be produced in higher purity than HMF and has higher stability[30,31]. We also demonstrated applications of HAH and hydrogenated HAH-derived monomers in the synthesis of performance-enhanced polyurethanes and polyester products with tunable properties.[30] Depending on the degree of hydrogenation and resulting monomer functionality, HAH-derived polymers showed improved thermal stability and stiffness to polymeric products, and could be used for UV-blocking and water resistant coatings and or energy-dissipating coatings for packaging. Furthermore, HAH derived monomers could be used for anti-microbial or controlled drug delivery when crosslinked by Diels-Alder coupling with bismaleimides.[30] HAH is fully conjugated along the symmetric furan-enone-bridge-furan backbone, and it contains various functional groups available for hydrogenation, specifically furan, ketone, and enone groups. **Scheme 1** depicts previously elucidated pathways for hydrogenation of HAH over Pd catalysts to various partially and fully hydrogenated products. As the C=C bonds in the enone bridge and furan rings are hydrogenated, more rotation and flexibility are imparted to the molecule. The degree of hydrogenation of HAH altered the physical and thermal properties of polymer products synthesized from these hydrogenated monomers.[30]

Previous investigations of the HAH hydrogenation reaction pathway over Pd did not selectively produce the fully hydrogenated product (FHAH=O or FHAH-OH, **Scheme 1**). This non-selective hydrogenation necessitates expensive separation and purification steps. Although PHAH=O and FHAH=O were selectively produced by varying temperature, solvent and residence time, the reaction kinetics are not well understood.[29]

Quantifying reaction kinetics allows for controlling product selectivity and expansion beyond HAH-derived monomer applications suitable for mixtures (currently confined to fuel and polymer additive industries) toward specialty chemical applications that drop into a wider array of polymer, pharmaceutical, and fuel applications. To address this challenge, we have investigated the selective hydrogenation of HAH to partially and fully hydrogenated monomers over Pd, Ru, and Cu catalysts. This work expands on the previously reported reaction scheme for HAH hydrogenation over Pd[29] and resolves reaction schemes over Ru and Cu catalysts. We suggest catalysts that can selectively produce target products (PHAH=O, FHAH-OH) and identify new intermediates and hydrogenated products that can be selectively targeted over each catalyst. We obtain lumped rate expressions to describe the hydrogenation of HAH and developed a kinetic model that describes experimental hydrogenation results. From this study, we investigate the optimized reaction conditions for controlled hydrogenation of HAH by calculating apparent rate constants, activation energies, and orders for the selective hydrogenation of HAH over Pd, Ru, and Cu surfaces.

Results

Catalysts Characterization

Metal loadings, the chemisorption uptake and the estimate dispersion for the catalysts used in this study are shown in Table 1. CO chemisorption was used to measure Pd and Ru surface sites. N_2O titration was used to measure the Cu surface sites. The metal loading of the ion exchange Cu catalyst was determined by ICP analysis. The metal loadings of the Pd and Ru catalysts are reported by the manufacturers. Dispersions were calculated assuming 100% reduction of the metal. All catalysts were pretreated under flowing inert and heated to 493 K prior

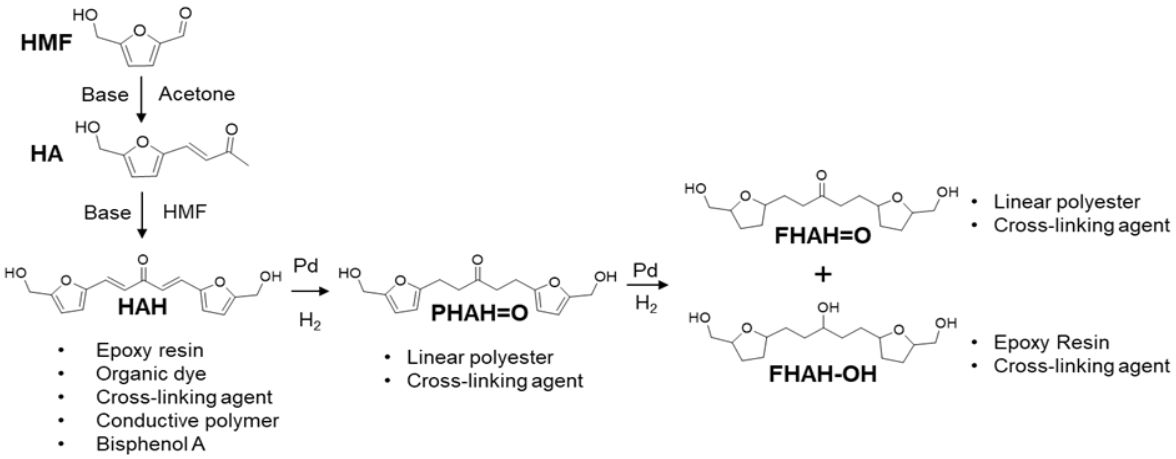

Scheme 1. Formation of HAH from Diels-Alder reaction of HMF and acetone, followed by Pd-catalyzed hydrogenation to various hydrogenation products. (adapted from 3)

to reduction and site quantification. The Pd catalyst was reduced at 313 K and the Ru catalyst was reduced at either 313 or 523 K to represent a less reduced (Ru-313) and a moderately reduced (Ru-523) surface. A higher reduction temperature was found to decrease the CO uptake and dispersion on the Ru surface. For the Cu pretreatment, a 573 K reduction was used before site measurement to match pretreatment before reaction with HAH. The Ru/C catalysts pretreated at 313 K exhibits the highest dispersion at 60%, followed by Cu and finally Pd with only 6% dispersion. We anticipate that the Pd may be highly dispersed on the alumina support, such that an inhibition of CO uptake occurs, as reported in the literature.[32] Temperature programmed reduction profiles for each catalyst are detailed in **Figures S1-S2.**

Reaction Kinetics Study and Model for HAH Hydrogenation

Table 1. Properties of Pd, Ru, and Cu catalysts.

Catalyst	wt.%	Reduction Temperature (K)	Chemisorption uptake (μmol/g)	Dispersion (%)
Pd/Al_2O_3	5	313	1.4	6.0
Ru-523/C	5	523	12.1	49
Ru-313/C	5	313	14.8	60
$Cu/\gamma\text{-}Al_2O_3$	3.6	573	8.6	15

Reaction kinetics experiments were carried out using a 45 mL Parr reactor equipped with a dip tube for sampling. Temperature was varied between 413 and 493 K. A simplified, lumped reaction scheme was developed to describe the hydrogenation of HAH within the reaction kinetics model, shown in **Scheme 2**. In steps 1-3, the hydrogenation follows a sequential mechanism where HAH is first converted to PHAH=O, and then further hydrogenated to FHAH=O and finally FHAH-OH. The first three sequential steps (**Scheme 2**, steps 1-3) represent lumped reactions that contain multiple mechanistic steps. As such, steps involving the addition of multiple hydrogen molecules (**Scheme 2**, steps 1 and 2) include derivatives of the final products in a step (**Figure S3**). These derivatives can be difficult to isolate and differentiate within complex mixtures, especially given the presence of isomers of the ring-containing products. For this reason, derivatives were either excluded from the analysis if they represented a significantly small fraction of the overall carbon balance (<10%) or were otherwise lumped in with the final product concentration of that step. Steps 4 and 5 represent parallel reaction pathways and describe direct hydrogenation from HAH to FHAH=O or FHAH-OH, representing a scenario where the binding of HAH and early hydrogenation products to the reactive surface is strong, such that partially hydrogenated products may not desorb before further

1. $HAH + 2\ H_2 \rightarrow PHAH{=}O$
2. $PHAH{=}O + 4\ H_2 \rightarrow FHAH{=}O$
3. $FHAH{=}O + H_2 \rightarrow FHAH\text{-}OH$
4. $HAH + 6\ H_2 \rightarrow FHAH{=}O$
5. $HAH + 7\ H_2 \rightarrow FHAH\text{-}OH$

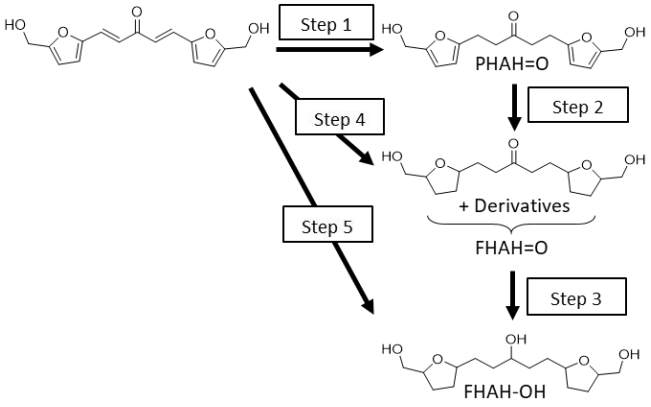

Scheme 2. Proposed reaction pathway over Pd and Ru:

conversion to more hydrogenated products. **Scheme 2** does not consider additional byproduct formation.

HAH Hydrogenation over Pd/Al_2O_3

Figure 1 displays concentration profiles for HAH hydrogenation over 5 wt% Pd/Al2O3 in isopropanol (IPA) solvent between 313-393 K. Over Pd, HAH is fully consumed at less than 20 minutes reaction time for all temperatures, and produces a mixture of PHAH=O, FHAH=O, and FHAH-OH products. The highest yield of PHAH=O over this surface is rapidly reached within 30 minutes and then consumed, indicating that it is directly produced from HAH before further conversion. The increase and decrease of the PHAH=O concentration embody the characteristic behavior of an intermediate product within a series that is converted to further hydrogenated products. Notably, FHAH=O is produced in over 70 mol% yields within the first 30 minutes of reaction, revealing that it is also directly produced from HAH. Final product distributions over all conditions examined show a mixture of FHAH=O and FHAH-OH, with FHAH=O as the primary product even at reaction times longer than 16 hours at 393 and 363 K. The FHAH-OH concentration remains comparably low (less than 22% yield) throughout all reaction times examined. Pd is known to have high activity in hydrogenation reactions[33], so the observed rapid conversion of HAH is expected and the final product mixture of FHAH=O and FHAH-OH reflects previous product mixtures after batch HAH hydrogenation over Pd in methanol.[29] An additional reaction intermediate, I-HAH (see **Scheme 3**), was observed in small concentrations over Pd at <10% of the carbon balance at only the earliest time point for 313 and 333 K reactions, and was therefore omitted from the kinetic model. Moreover, exclusion of I-HAH did not significantly affect the concentration profiles or model fits.

The Akaike Information Criterion (AIC) was used to determine the optimal fit between a sequential 3-step scheme (consisting of steps 1, 2, and 3) and the 5-step reaction scheme (**Scheme 2**). The AIC compares the residual error of fits and selects for the closest fitting model with the least amount of added fitting parameters to prevent overfitting of the dataset.[34] Statistical analysis by the AIC parameter indicated that the 5-step reaction scheme best fit the experimental data (**Table S1**). We note that without the presence of an active catalyst, only 10% conversion of HAH was observed after 12 h of reaction time at 120˚C in IPA, yielding an unknown product that is attributed to thermal degradation (**Figure S5**).

HAH Hydrogenation over Ru/C

A 5 wt% Ru/C catalyst was examined in the hydrogenation of HAH. **Figure 3** depicts the concentration profiles of hydrogenation over Ru-523/C (Ru/C catalyst that underwent prior reduction at 523 K) throughout a temperature range of 313 – 393 K. HAH was hydrogenated to a mixture of PHAH=O, FHAH=O, and FHAH-OH, where PHAH=O exhibited behavior consistent with a reaction intermediate. The fit of the reaction kinetics model shows a reaction pathway consistent with **Scheme 2**, where all consecutive and parallel steps are active

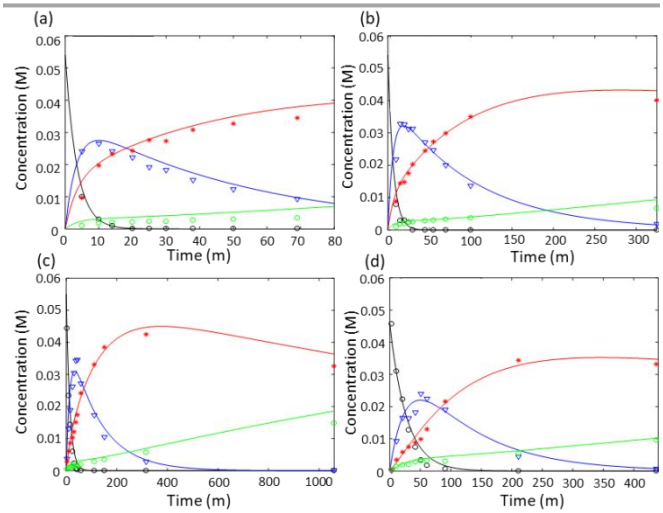

Figure 2. Concentration profiles of HAH and hydrogenation products over 5 wt% Ru-313/C as a function of temperature. (a) T = 393 K, (b) T = 363 K, (c) T = 333 K, (d) T = 313 K. Other conditions and labels for experimental data and kinetic model identical to **Figure 1**.

(**Table S1**). First order dependencies of HAH and the hydrogenated products were found to best fit experimental data. I-HAH was omitted from the kinetic model as it represented less than 10% of the carbon at the earliest reaction time points over Ru catalysts. The small amounts of reaction intermediates and byproducts are again reflected by the close fits between model and experimental data.

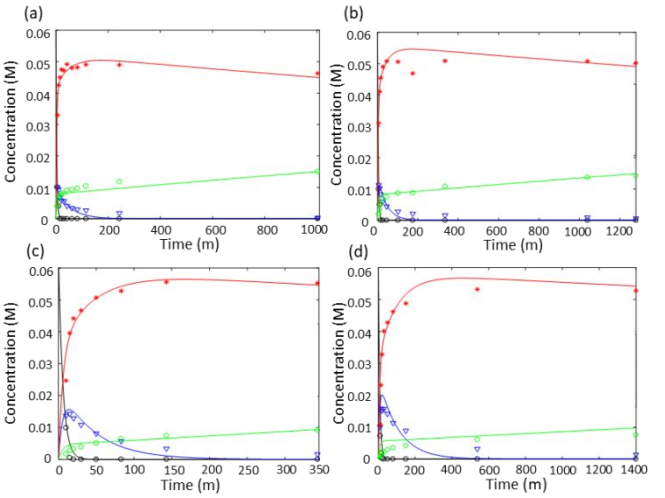

Figure 1. Hydrogenation of HAH over Pd/Al_2O_3 at different temperatures. (a) T = 393 K, 20 mg catalyst, (b) T = 363 K, 30 mg catalyst, (c) T = 333 K, 30 mg catalyst, (d) T = 313 K, 30 mg catalyst. Other conditions: 460 mg HAH in 30 mL IPA, and 30 bar H_2 (room temperature). Points denote experimental data, and solid lines represent the kinetic model (conversion and selectivity trajectories). (Black: HAH, blue: PHAH=O, red: FHAH=O, green: FHAH-OH. Errors are typically less than 0.003 M, as shown in **Figure S4.**)

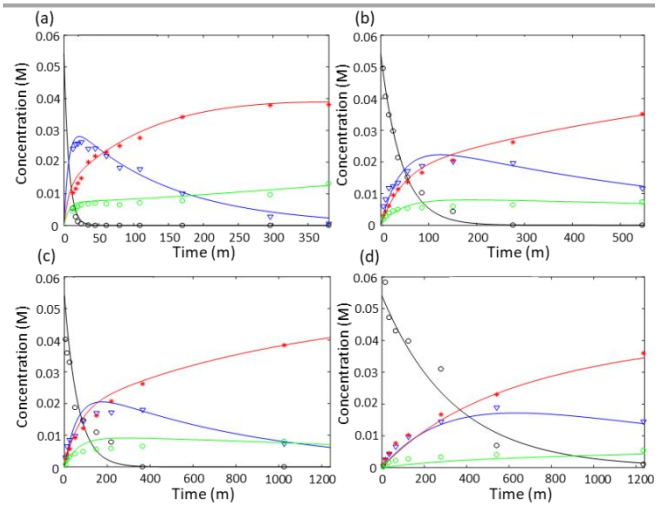

Figure 3. Concentration profiles of HAH and hydrogenation products over Ru-523/C at different temperatures. (a) T = 393 K, 30 mg catalyst, (b) T = 363 K, 25 mg catalyst, (c) T = 333 K, 30 mg catalyst, (d) T = 313 K. Ru-523/C was reduced at 523 K for 3 h under 58 bar H_2 prior to reaction. Other conditions and labels for experimental data and kinetic model identical to **Figure 1**.

A series of reaction kinetics experiments on Ru-313/C (Ru/C that did not go a prior reduction treatment before reaction) were then carried out to determine the effect of reduction on Ru in HAH hydrogenation. **Figure 2** demonstrates the close model agreement with the experimental data over the Ru/C catalyst for all temperatures examined. PHAH=O is the first dominant hydrogenation product that desorbs from the catalyst and can be produced in up to 63% yields before re-adsorbing to form FHAH=O, which becomes the next dominant hydrogenation product (up to 77% yield).

HAH Hydrogenation over Cu/Al_2O_3

Results of HAH hydrogenation over Cu/Al_2O_3 are shown in Figure 4. Hydrogenation over Cu showed a slower reaction rate than both Pd and Ru. Additionally, reaction over Cu yielded intermediate I-HAH in significant concentrations, comparable to the concentrations of PHAH=O over Ru and Pd catalysts. The Cu catalyst was inactive for hydrogenation of the furan rings and subsequent production of FHAH=O and FHAH-OH. NMR spectra identifying I-HAH and PHAH-OH are shown in **Figures S8-S9** and **Figures S10-S11**, respectively.

1a. HAH + H_2 → I-HAH

1b. I-HAH + H_2 → PHAH=O

6. PHAH=O + H_2 → PHAH-OH

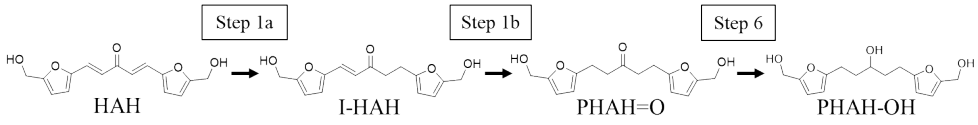

Scheme 3. Proposed reaction pathway over Cu:

Hydrogenation over Cu terminated in a new triol product from previous schemes, PHAH-OH (**Scheme 3**). We suggest a separate, 3-step reaction pathway with an additional intermediate and new fully hydrogenated product. The three lumped steps shown in **Scheme 3** were used to fit the reaction kinetics data over the Cu catalyst.

We note that this reaction path consists only of sequential hydrogenation steps, unlike the behavior observed over Ru and Pd catalysts. A 5-step scheme was also examined where parallel steps to PHAH=O and PHAH-OH were considered, but a comparison of fit using the AIC gave similar effectiveness of fit, and the 5-step mechanism yielded unrealistic rate constants. Therefore, the 5-step scheme showed little benefit over the 3-step pathway over Cu (**Table S1**). The sequential behavior can be seen by the lack of FHAH-OH produced at initial time points over Cu, visible in **Figure 4**. **Scheme 3** shows that HAH is first converted to intermediate I-HAH before sequential conversion to product PHAH=O. Hydrogenation over Cu exhibited near full conversion of HAH to I-HAH for reactions at 313 and 333 K as the first major hydrogenation product. At the lowest temperature conditions examined (333 K), a 61% yield of I-HAH was achieved after 22 h reaction time. Additionally, PHAH=O was selectively produced at yields of 85% at multiple reaction temperatures examined. The high selectivity to partially hydrogenated monomers over Cu is likely due to the lack of parallel pathways, which contribute to higher concentrations of more saturated products present in Ru-313/C (63% yield PHAH). We note that higher amounts of dehydrated byproducts were observed over the Cu catalyst compared to Ru and Pd, and that high temperatures (393 K) yielded more dehydration products. However, excluding these byproducts from the concentration profiles yielded carbon balances above 86 % for temperatures 313, 333, and 363 K and an 82% carbon balance for reaction at 393 K. These carbon balances were sufficient for model fitting and reaction kinetics analysis.

Reaction Orders, Combined Scheme, Apparent Activation Energies

The reaction orders of HAH and hydrogen were experimentally determined in a batch system over Pd/Al_2O_3, Ru/C, $Cu/\gamma\text{-}Al_2O_3$ catalysts. **Table 2** shows orders close to one for HAH and H_2, suggesting first order dependence with respect to HAH and hydrogen over Pd, Ru, and Cu catalysts. We note that the reaction order with respect to the hydrogen partial pressure was calculated from the HAH consumption, and represents a lumped order combining steps 1, 4, and 5. Reaction conditions correspond to those shown in **Figure S7.**

Table 2. Comparison of reaction orders for HAH and hydrogen over 5 wt% Pd/Al_2O_3, 5 wt% Ru/C, and 3.6 wt% Cu/Al_2O_3. Errors shown are 90% confidence intervals.

Reaction order	HAH	H_2
Pd/Al_2O_3	0.86 ± 0.26	1.16 ± 0.004
Ru/C	0.85 ± 0.20	1.26 ± 0.25
Cu/Al_2O_3	1.08 ± 0.01	1.09 ± 0.003

A general HAH hydrogenation reaction scheme is depicted in **Scheme 4**. Over Pd and Ru, HAH is hydrogenated in the enone bridge through intermediate I-HAH to the first major hydrogenation product, PHAH=O. Next, hydrogenation at the furan rings yields FHAH=O. FHAH=O is the major product over Pd, but further hydrogenation can occur over both Pd and Ru surfaces to the fully hydrogenated product, FHAH-OH. However, FHAH-OH can only be selectively produced over the Ru catalyst. Over the Cu catalyst, the HAH enone bridge is partially hydrogenated, yielding intermediate I-HAH as the first primary product. Further hydrogenation completes the second enone C=C hydrogenation and selectively produces PHAH=O. Finally the reaction terminates to the triol, PHAH-OH without hydrogenation of the furan rings.

Table 3 shows a comparison of the apparent activation energies of each of the HAH hydrogenation pathways over Pd, Ru, and Cu catalysts calculated from rate constants derived from the reaction kinetics model. Over Pd/Al_2O_3, the initial hydrogenation of the enone bridge C=C bonds is almost barrierless. The barrier for steps 4 and 5 (**Scheme 4**) are also low, albeit significantly higher than that of step 1. Notably, the sequential step 3 is essentially inactive over Pd at the time scales examined, leading to a fully converted product mixture of FHAH=O and FHAH-OH and a parallel pathway scheme. Activation energies are significantly higher over Ru-523/C, supporting the slower reaction rates observed over Ru. Additionally, step 3 in **Scheme 4** is more active and full conversion of HAH to FHAH-OH is feasible at sufficiently long reaction times (>24 h at 393 K). Omitting the 523 K reduction step for Ru/C causes a decrease in the energy barrier of the first two sequential pathway steps (converting HAH to PHAH=O and then FHAH=O). The energy barriers over $Cu/\gamma\text{-}Al_2O_3$ are generally higher than those over both Ru catalysts and Pd. The first step is split into two separate lumped reactions, forming I-HAH and PHAH=O as major products separately. Additionally, the terminal step over Cu ends in a separate final product with a similarly high energy barrier.

Table S2 depicts optimized rate constants fit to each scheme step over all catalysts examined at a reference temperature of 333 K. The fastest rate constants can be seen over the Pd catalyst for each step in the Pd/Al_2O_3 scheme (**Scheme 4**). The

Table 4. Optimized product yields from kinetic model for PHAH=O, FHAH=O, FHAH-OH, I-HAH, and PHAH-OH over 313 – 393 K temperature range over Pd, Ru, and Cu catalysts in a 30 mL batch reactor. Optimal yields of less than 30 % are not shown.

Catalysts		I-HAH	PHAH=O	PHAH-OH	FHAH=O	FHAH-OH
Pd	Yield (%)	-	-	-	92	-
	T (K)	-	-	-	313	-
	t (min)	-	-	-	190	-
	m_{cat} (g)	-	-	-	0.10	-
Ru-523	Yield (%)	-	50	-	75	99
	T (K)	-	393	-	393	393
	t (min)	-	25	-	30	600
	m_{cat} (g)	-	0.03	-	0.50	1.0
Ru-313	Yield (%)	-	56	-	82	99
	T (K)	-	393	-	393	393
	t (min)	-	56	-	78	290
	m_{cat} (g)	-	0.01	-	0.06	0.75
Cu	Yield (%)	51	79	99	-	-
	T (K)	313	393	393	-	-
	t (min)	130	120	300	-	-
	m_{cat} (g)	1.0	0.1	1.0	-	-

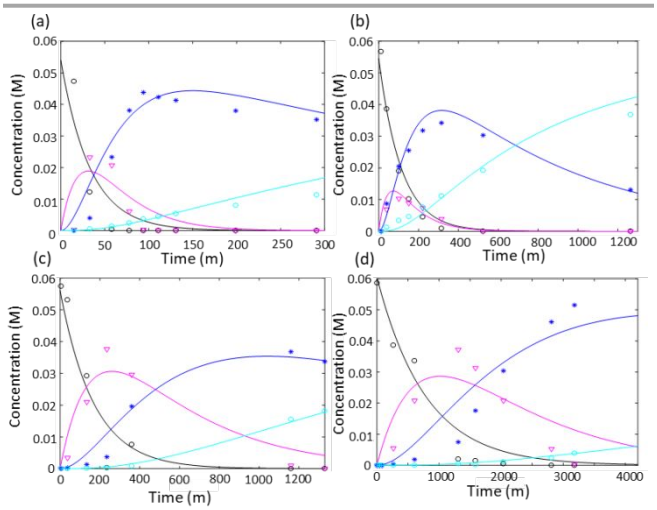

Figure 4. Hydrogenation of HAH over $Cu/\gamma\text{-}Al_2O_3$ at different temperatures. (a) T = 393 K, 100 mg catalyst, (b) T = 363 K, 100 mg catalyst, (c) T = 333 K, 150 mg catalyst, (d) T = 313 K, 150 mg catalyst. Cu was reduced at 573 K for 5 h under 63 bar H_2 prior to reaction. Other conditions and identical to **Figure 1**. (Black: HAH, magenta: I-HAH, blue: PHAH=O, cyan: PHAH-OH. See **Scheme 3** for product structures.)

Table 3. Model calculated apparent activation energies for the 4-step pathway over Pd/Al_2O_3 (no pretreatment), 5-step reaction pathway over Ru-523/C (reduced at 523 K for 1 h) and Ru-313/C (no pretreatment), and a 3-step reaction pathway over $Cu/\gamma\text{-}Al_2O_3$ (reduced at 573 K for 5 h) catalysts from 313 to 393 K.

Steps		Pd/Al_2O_3 E_{Ap} (kJ mol^{-1})	Ru-523/C E_{Ap} (kJ mol^{-1})	Ru-313/C E_{Ap} (kJ mol^{-1})	$Cu/\gamma\text{-}Al_2O_3$ E_{Ap} (kJ mol^{-1})
1a	HAH → I-HAH	2.8 ± 0.8	46 ± 16	30 ± 12	43 ± 14
1b	I-HAH → PHAH=O	-			58 ± 26
2	PHAH=O → FHAH=O	17 ± 14	30 ± 14	15 ± 8	--
3	FHAH=O → FHAH-OH	--	14 ± 11	15 ± 4	--
4	HAH → FHAH=O	7.8 ± 4.7	37 ± 13	43 ± 15	--
5	HAH → FHAH-OH	11 ± 8.0	44 ± 19	24 ± 3	--
6	PHAH=O → PHAH-OH	--	--	--	41 ± 26

next highest rate constants are seen over the untreated Ru catalyst. Again, Cu exhibits the lowest rate constants observed. We then used the kinetic model to predict optimized product yields using the kinetic data from the Arrhenius plots shown in **Figures S12 - S15. Table 4** shows the optimized yields in 30 mL batch reactors and the corresponding reaction conditions for the hydrogenation product over Pd, Ru, and Cu within the studied temperature range (313 – 393 K). When optimized conditions over a given catalyst yielded less than 30 % of a desired product, no optimal yield was listed. In these cases, the catalyst is considered a poor candidate for production of the hydrogenated molecules in question. Catalyst weights were varied such that reaction times were typically less than 5 h.

Figure 5 depict the optimized yields of each hydrogenation product (described in **Table 4**) along a universal x-axis, $X_{Batch\ /\ PFR}$, derived from batch and plug flow reactor (PFR) design equations in Eqn. 1 and Eqn. 2:

Eqn. 1 $$\frac{dC_i}{dt} = \left[\frac{m_{Batch}}{V_R}\right]\sum_j k_j f_j(C_k)$$

Eqn. 2 $$\frac{dC_i}{d(z)} = \left[\frac{m_{PFR}}{v_{liq}}\right]\sum_j k_j f_j(C_k)$$

where t represents the time in the batch reactor (min), m_{Batch} and m_{PFR} represent the total mass of catalyst used in the batch and PFR reaction, respectively (g), and V_R and v_{liq} are the volume of the liquid volume of the batch reactor (L) and the liquid flow rate in the PFR (L min^{-1}). Finally, z is the mass of the catalyst bed reacted normalized by the total mass of the bed. As such, z is equal to 1 at the outlet of the PFR reactor bed. By integrating and equating Eqn. 1 and Eqn. 2, we can derive a

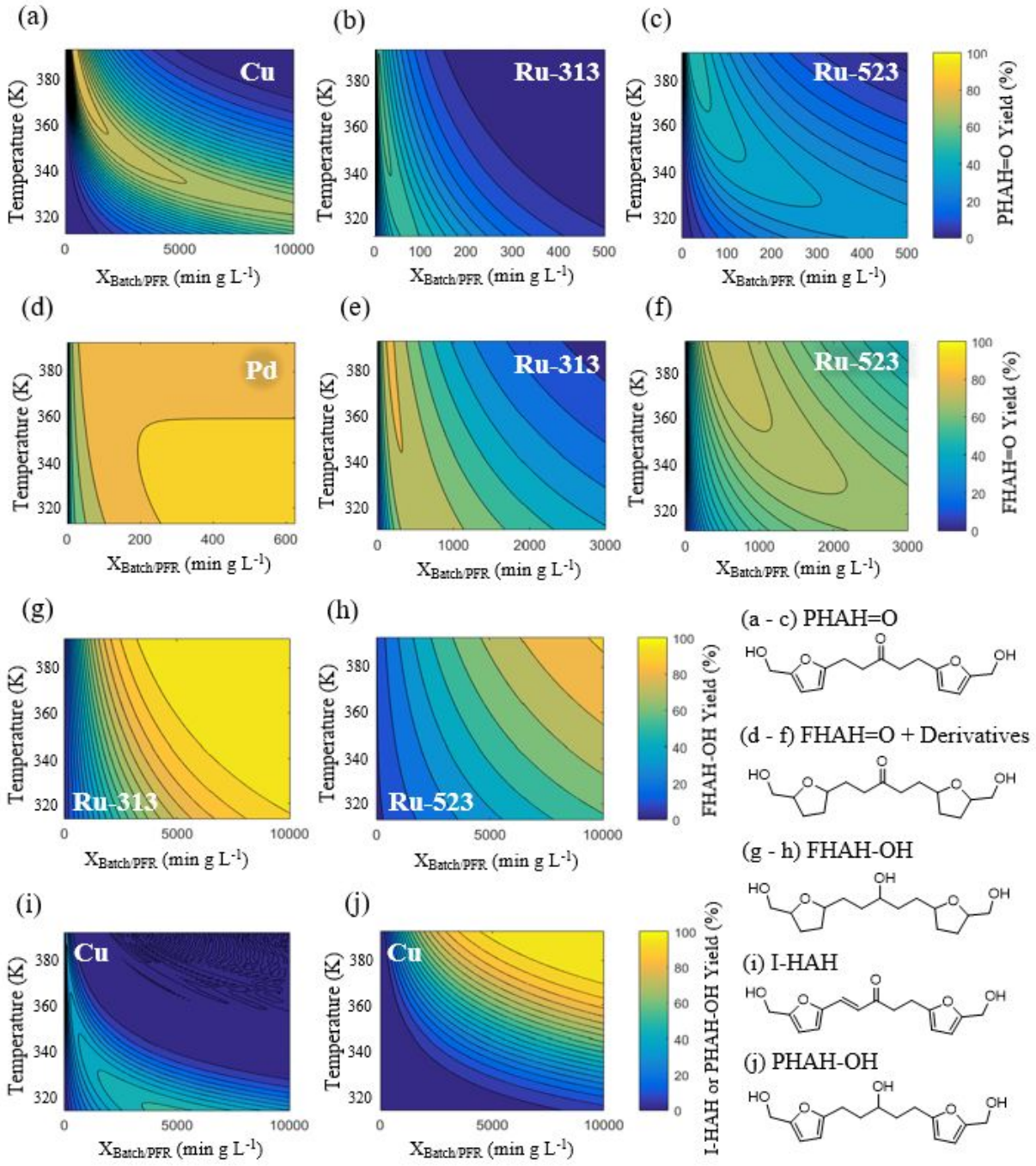

Figure 5. Universal yield plots for optimized production of (a – c) PHAH=O, (d – f) FHAH=O and derivatives, (g – h) FHAH-OH, (i) I-HAH, and (j) PHAH-OH in batch and plug flow reactors from 313 – 393 K over Pd/Al_2O_3, Ru/C (Ru-313 or Ru-523), and Cu/Al_2O_3 catalysts. Maximum yields of PHAH=O over: (a) Cu/Al_2O_3 at 393 K, (b) Ru-313/C at 363 K, and (c) Ru-523/C at 393 K. Maximum yield of FHAH=O and derivatives over: (a) Pd/Al_2O_3 at 313 K, (b) Ru-313/C at 393 K, and (c) Ru-523/C at 393 K. Maximum yield of PHAH-OH over: (a) Ru-313 and (b) Ru-523 at 393 K. Maximum yield of I-HAH and PHAH-OH over Cu/Al_2O_3 at 313 K and 393 K, respectively. All reactions were loaded with 0.056 M HAH and 30 bar H_2.

simple equation for $X_{Batch\ /\ PFR}$, representing either a function of time in a batch reactor or the total weight ratio of a plug flow reactor, as shown in **where** :

Eqn. 3 $$\frac{dC_i}{dXBatch/PFR} = \sum_j k_j f_j(C_k)$$

where $$X_{Batch\ /\ PFR} = t\frac{m_{Batch}}{V_R} = z\frac{m_{PFR}}{\upsilon_{liq}}$$

Figure 5 sizes the reactor or determines the required flow rate and catalyst weight for a batch or PFR system at the optimal conditions to produce hydrogenated HAH monomers of interest over the optimal catalyst, per the reaction kinetics parameters determined from this study. From the optimal yield results, PHAH=O was found to be produced with moderate-to-high selectivity over Cu and both Ru catalysts. The maximum PHAH=O yield is visible in **Figure 5a**, which shows a yield of 78.7% PHAH=O at $X_{Batch\ /\ PFR} = 415$ min g L^{-1} over Cu/Al_2O_3 at 393 K. Ru-313/C yielded higher predicted maximum PHAH=O (56%) than the optimal PHAH=O yields predicted over Ru-523/C (50 %) in the examined temperature range. FHAH=O and corresponding derivatives were predicted to have a maximum combined yield over Pd (92.2% at 313 K). The yield was found to increase with decreasing temperature. This prediction was close to the experimentally observed yield over Pd of 85% at 313 K. In the universal yield plot in **Figure 5(d)**, this maximum yield occurs at $X_{Batch\ /\ PFR} =$ 625 min g L^{-1}. FHAH=O and its derivatives were also yielded over both Ru catalysts. Yields are predicted to increase with temperature over Ru-523/C and Ru-313/C, and reach maxima of 75.1% and 81.6%, respectively, at 393 K. However, Ru-313/C was more active, as seen when comparing the time scales of **Figure 5(e)** and (**f)**, yielding maximum FHAH=O at $X_{Batch\ /\ PFR} =$ 155 min g L^{-1}. **Figure 5(g)** and **(h)** shows that FHAH-OH was predicted to achieve ~100 % yield over both Ru catalyst as the final product in the sequential hydrogenation reaction scheme. However, faster production with lower catalyst weights was predicted over the untreated Ru/C compared to Ru/C after reduction. FHAH-OH production over Ru-313/C was optimized at 99.9% yield at $X_{Batch\ /\ PFR} =$ 7250 min g L^{-1}. While full conversion of HAH to FHAH-OH is possible at low temperatures, higher temperatures afforded shorter reaction times, and suffered little penalty of degradation reactions, as few unknown compounds were observed over Ru catalysts throughout the investigated temperature range (313 – 393 K). Two additional compounds were identified in this study over the Cu/Al_2O_3 catalyst. I-HAH was produced in lower but moderately selective yields (51%). Low temperatures were found to favor higher I-HAH yields. Cu/Al_2O_3 was also the only catalyst that yielded PHAH-OH. PHAH-OH yields were found to increase with increasing temperature. PHAH-OH yields were optimized at $X_{Batch\ /\ PFR} =$ 9900 min g L^{-1}, yielding 99.9% conversion to the final hydrogenation product along the reaction scheme over Cu.

We note that the optimized product selectivities represent the optimized values for the specific catalysts examined in this work, since factors such as metal dispersion and textural properties of the support are expected to play a role in the reaction kinetics of the reaction, as evidenced by other hydrogenation studies with similar catalysts in the literature.[35-37] However, these properties are not expected to significantly affect the thermodynamics and overall mechanism of the hydrogenation. These factors are outside the scope of this work and are of interest for future work.

Discussion

The reaction kinetics model was used to fit the concentration profiles over the Pd/Al_2O_3 catalyst and showed close agreement to the experimental data in **Figure 1** at each temperature examined. Pd/Al_2O_3 exhibits a 4-step, lumped reaction pathways consisting of steps 1, 2, 4 and 5 in **Scheme 2**. The model results describe hydrogenation over Pd as dominated by the parallel paths (steps 4 and 5), converting HAH directly to products FHAH=O and FHAH-OH. We suggest that the low selectivity over Pd toward PHAH=O (< 25% yield) at early reaction times is due to strong binding of the reactive intermediates to the Pd surface, leading to rapid, unselective hydrogenation before desorbing. Literature studies have reported similar strong interaction of species containing furan rings to Pd. The strong binding is attributed to an sp^2 to sp^3 rehybridization as the π bonds in the furan ring interact with the *d*-band of the Pd surface, allowing an essentially flat adsorption configuration of the planar ring.[33,38] This behavior is further evidenced by the direct conversion of HAH to FHAH=O and FHAH-OH products at the beginning of the hydrogenation. Moreover, the model fits showed rate constants for step 3 at or near zero (<0.0001 L min^{-1} g $^{-1}$), representing little to no flux through the pathway where FHAH=O is converted to FHAH-OH. Accordingly, once FHAH=O is formed as the major reaction product and desorbs from the Pd surface, it does not undergo further adsorption and hydrogenation in the time scales examined. In the literature, the rehybridization of sp^2 C-C bonding in furan to sp^3 has been reported to push the furan O atom sufficiently away from the surface of Pd, such that the O-Pd bond interaction is small.[38] This hypothesis supports the low conversion to the fully hydrogenated FHAH-OH product (<22% yield), and offers explanation to the lack of further hydrogenation of FHAH=O products to FHAH-OH. Varying final product ratios can be achieved by adjusting the reaction temperature, ranging from molar ratios of 7:1 to 3:1 of FHAH=O to FHAH-OH from 313 to 393 K, respectively. This tunable final product ratio likely reflects stronger binding of the conjugated π bonds to the Pd surface as temperature is increased.

Despite significant side reactions often reported for hydrogenation reactions over Pd surfaces,[23,39,40] minimal side products were observed over Pd/Al_2O_3, contributing to the close agreement between experimental data and modelled fits in **Figure 1**. In DFT studies over Pd,[41] H-covered surfaces have been reported to introduce a tilt in adsorbed furanyl and furfural rings, subsequently weakening the binding of furan to Pd. This tilt was suggested to increase barriers for undesirable side reactions like decarbonylation and ring opening,[41] thereby shifting reactivity toward hydrogenation pathways. It is possible

that the high hydrogen pressures used in these experiments promote a H-covered Pd surface that contributes to the lack of hydrodeoxygenation, decarbonylation, and ring opening products that are otherwise observed over Pd surfaces during furfural, FA, and FAF hydrogenations reactions.[23,39,40]

In contrast to the Pd/Al_2O_3 catalyst, Ru-523/C was less active and produced lower PHAH=O and FHAH=O concentrations at the initial reaction time points. Similar results were reported in a study of furfural hydrogenation over 3 wt% Ru/C at 35 bar and 493 K, which showed that Ru/C displayed exhibited lower activity than Pd based catalysts (quantification of sites was not performed). However, the Ru/C catalyst showed significantly lower activity than the Ru-523/C catalyst examined here: only 57% conversion of furfural after 5 h of reaction time with 18% yield to furfuryl alcohol, a partial hydrogenation product, and 23% yield to tetrahydrofurfuryl alcohol, the fully hydrogenated product.[42] Other reports in the literature have suggested that Ru is structure sensitive for hydrogenation reactions, where stronger interaction of Ru with the support facilitates higher dispersion and subsequently higher hydrogenation activities.[33] The commercial Ru/C catalyst used in this work has a high dispersion (60%) after reduction at 523 K, likely contributing to higher activity seen in this study. Comparing **Figure 1** and **Figure 3**, roughly twice the intermediate concentrations of PHAH=O were achieved compared to over Pd/Al_2O_3, and the selectivity toward PHAH=O as the first major product was observed to increase with reaction temperature (from ~35 to 50% yield from 313 to 393 K). PHAH=O and FHAH=O products were typically produced in near equimolar yields over short reaction times. **Figure S6** shows that FHAH=O products are observed to reach a maximum concentration and subsequently decrease. Accordingly, FHAH=O is labelled an intermediate product within the hydrogenation of HAH over Ru, in contrast to a final product over Pd.

In **Figure 2**, the selectivity toward FHAH-OH over Ru-313/C increases gradually in the first 30 minutes of the reaction, and the yields of FHAH=O and FHAH-OH at early reaction times are considerably lower than over Ru-523/C. This likely indicates a weaker binding over the Ru-313/C surface compared to Ru-523/C surface. However, small amounts of FHAH=O and FHAH-OH are still produced at the start of the reaction, evidencing the presence of the parallel steps 4 and 5 in **Scheme 2**. The agreement of model fits between Pd and all Ru experiments demonstrates that the reaction pathway remains the same over each catalyst, while only the fluxes through the pathways change. The hydrogenation proceeds faster over the lesser reduced Ru surface (Ru-313/C), yielding similar product distributions for reaction at 393 K over 30 mg Pd/Al_2O_3 at 160 min for Ru-523/C vs. 80 min for Ru-313/C, respectively. As such, Ru-313/C models show shorter reaction times to the final hydrogenation product compared to Ru-523/C and Pd/Al_2O_3. Similar selective conversion to the final hydrogenation product was reported for furfural hydrogenation over a mildly reduced Ru catalyst, where the reduction of 2 g of RuO_2 at 330 – 350 K yielded 89% tetrahydrofurfuryl alcohol after 95 minutes at 50 bar H_2, at 393 K in methanol.[43]

A comparison of the effects of Ru/C pretreatment indicates that the more reduced Ru surface favors parallel pathways (steps 4 and 5 in **Scheme 2**), likely due to an increase in binding strength of furan ring π bonds with Ru^0, leading to further hydrogenation of bound species prior to desorption, as seen over the Pd catalyst. As such, Ru-313/C is a more selective and more active candidate than Ru-523/C or Pd to produce PHAH=O and FHAH-OH over 313 – 393 K.

HAH and the subsequent hydrogenation products may bind differently to Cu due to the filled *d*-shell, in contrast to the unfilled *d*-shells of Pd and Ru which promote stronger interaction with the furan rings.[41] Similar low activity for the hydrogenation of furan rings has been noted in experimental studies of furan over Cu(100), which demonstrate that furan adsorbs and desorbs from the Cu surface intact.[44] One study of furfural hydrogenation over Cu/SiO_2 attributes the lack of conversion in the furan rings to a partial overlap of the full 3d band with the antibonding orbitals of the aromatic furan ring.[15] This overlap results in repulsion of the furan ring from the Cu surface, preventing a flat adsorption configuration. Instead, the most stable adsorption configuration of furfural to Cu is suggested to be a η^1(O)-aldehyde binding mode (perpendicular or tilted configuration) through the carbonyl group O lone pair of electrons.[15,45,46] A similar repulsion of the furan ring was found over Cu during HMF adsorption, with the most stable binding occurring through the O group.[47] We anticipate that a similar overlap could prevent HAH from binding in a flat configuration, leading to weaker binding through the O atoms and the observed inactivity of HAH to fully hydrogenated products over Cu. The suggested perpendicular binding mode of HAH would support a slower, more selective hydrogenation of the enone groups within HAH.

A slight overestimation of the model fit over Cu (**Figure 4**) was obtained compared to the experimental data at the highest temperatures. Specifically, in **Figure 4 (a-b)**, the model overestimates the experimental concentration of PHAH=O and PHAH-OH at long reaction times. For the low temperatures at long reaction times, the model shows good agreement to experimental data for PHAH=O and PHAH-OH. This trend is consistent with lower carbon balances observed at higher temperatures, due to increased formation of byproducts at elevated temperatures. Despite this byproduct formation, our results identify the Cu/Al_2O_3 catalyst as the most selective catalyst for production of less saturated monomers like intermediate I-HAH and PHAH=O compared to Ru and Pd over 313 - 393 K. This increased selectivity is attributed to the binding configuration over Cu and lack of parallel reaction steps in the sequential hydrogenation scheme (**Scheme 3**).

The experimental results for order determination of HAH in **Figure S7** support a first order dependency for the HAH-derived products in the reaction kinetics analysis. As such, all additional hydrogenation monomers were assumed to be first order. This assumption is in agreement with literature for similar hydrogenation reactions of HMF[13], FA[23], and FAF[24]. When comparing apparent activation energy barriers in **Table 3**, the near barrierless hydrogenation of the C=C bond in the enone bridge over Pd/Al_2O_3 explains the rapid conversion (>95 mol%

conversion at 20 min) of HAH observed over the Pd hydrogenation profiles. The reduced energy barriers for steps 1 and 2 over Ru-313/C (compared to Ru-523/C) support the increased reaction rate constants observed over Ru-313/C compared to Ru-523/C (e.g., from 0.0532 vs. 0.0074 L min^{-1} g^{-1} for step 1 in **Table S2**), as well as the increased dependence on consecutive steps observed from the fitted reaction kinetics models. The high energy barriers determined over Cu/γ-Al_2O_3 for steps 1a, and 1b, and 6 (>40 kJ mol^{-1}, **Table 3**) reflect the lower activity observed for this catalyst compared to the other surfaces examined. In future studies, it will be useful to identify physical properties to describe the reactivity trends,[48] and we plan to carry out density functional theory studies to explore the reactivity trends observed in terms of surface binding energies and transition states.

In **Figure 5**, the plot of optimal PHAH=O yield suggests that temperatures above 393 K increase PHAH=O yields further over Cu/Al_2O_3, although we note the experimentally observed presence of unknown species at 393 K, potentially due to dehydration. While Ru-313/C produces slightly higher PHAH=O yields than Ru-523/C (56% vs. 50% yield, respectively, PHAH=O yields over Ru-523/C were found to increase with increasing temperature, while the yield over Ru-313/C reached a maximum at 363 K. This behavior suggests that Ru-523/C may be a promising candidate for production of PHAH=O at temperatures above 393 K. Future experimentation is needed to more accurately predict optimal yields at temperatures higher than 393 K. Selective production of PHAH=O is of particular interest for use as a functional polymer, and was successfully incorporated into blended polyurethanes experimentally.[30] This addition provided maleimide-appending sites for further Diels-Alder reactions. Our findings for the optimization of PHAH=O production also open research avenues into further applications such as for linear polyesters and cross-linking agents, as suggested in previous work from our group.[29] More research is needed to improve the yield of PHAH=O beyond the predicted maximum yield over the Cu/Al_2O_3 catalyst from conditions examined here. Meanwhile, for production of another partially hydrogenated intermediate compound, I-HAH over Cu in **Figure 5 (i)**, further investigation is required to achieve yields over 50%, since lowering the reaction temperature below 313 K is not practical.

Although Pd/Al_2O_3 produced higher FHAH=O yields than Ru-313/C (92 vs. 82% yield, **Figure 5 (g – h)**) at the optimized reaction conditions, Ru-313/C is also recommended for synthesizing FHAH=O products due to the trend of increasing yields at higher reaction temperatures above 393 K. This trend suggests that high temperature reactor studies would be promising for further research into selective FHAH=O production over Ru/C, since few side products were observed experimentally at 393 K. Similarly to PHAH=O, FHAH=O related products can also be implemented in linear polyurethane[30] and potentially in linear polyesters or as a cross-linking agent.[29]

Conditions to selectively produce the two final hydrogenation products, FHAH-OH and PHAH-OH, over Ru and Cu catalysts were determined, and near quantitative yields are predicted for each product. This opens many avenues for further research into numerous applications. For example, the free-rotation of sp^3 carbons in FHAH-OH contributed to high flexibility within a polymer structure that incorporated FHAH-OH, and resulted in an energy-dissipating rubber, despite HAH-based polyurethanes exhibiting stiffness.[30] The symmetric triol structure of FHAH-OH and PHAH-OH are anticipated to be useful for applications like cross linking agents and epoxy resins. Since PHAH-OH is structurally similar to PHAH=O, PHAH-OH can also be active for further Diels Alder reaction chemistry, opening pathways for investigation of this compound in functional polymer applications.

Overall, the results of the reaction kinetics model agree with experimentally observed optimal conditions and show similar maximum yields for each hydrogenation product examined. Additionally, the model provides further insight into promising temperature regions for future kinetic analysis that can produce higher selectivities of intermediate products like PHAH=O and FHAH=O. The reaction kinetics analysis also serves as the basis to future scale up of the selective hydrogenation of HAH to various monomer products over Pd, Ru, and Cu, allowing further research on these monomers as precursors to polymer chemistry applications.

Experimental Methods

Materials

HMF (98%, AK Scientific), acetone (HPLC grade, Fisher Scientific), NaOH (FCC specification, Fisher Scientific), HCl (37 wt.% Sigma-Aldrich), 2-propanol (HPLC Plus grade, Sigma-Aldrich), 5 wt.% Pd/Al_2O_3 (Strem Chemicals), 5 wt. % Ru/C (Aldrich), low soda gamma alumina (γ-Al_2O_3, Strem Chemicals), tetraaminecopper(II) sulfate ($[Cu(NH_3)_4]SO_4 \cdot xH_2O$), H_2SO_4 (95-98%, Sigma Aldrich), 18 Ohm Milli-Q water, H_2 (Industrial, Airgas) and Ar (Industrial, Airgas) were used as received. All reactions were carried out in a 50 mL Parr reactor (Parr Instrument Company) equipped with a dip tube for sampling during reaction.

HAH synthesis

HAH was synthesized following methods described elsewhere.[30] In brief, 10.25 g of HMF was added to 71.28 mL of 18 MΩ Milli-Q water and 3 mL acetone in a 500 mL round bottom flask. The mixture was heated to 35 ˚C and 6.67 mL 3 M NaOH was added. The mixture was stirred for 1 h and then removed from heat and neutralized with 3M HCl solution. Solid HAH precipitate was vacuum filtered and washed with excess water before drying in a 50 ˚C vacuum oven overnight.

HPLC analysis of HAH

High performance liquid chromatography (HPLC) was used to quantify the concentration of HAH in reaction solutions. Solutions containing HAH were diluted 600 times with IPA to ensure a measurable range of absorbance. All samples were filtered through 0.2 µm PTFE syringe filters prior to injection into the HPLC. The HPLC was equipped with a Luna C18(2) (Phenomenex Inc., part no. 00G-4252-E0) column set to 323 K and a Waters 2998 PDA detector set to 390 nm. A gradient

methanol/0.1 wt.% formic acid solution was used as the mobile phase at a of 1.0 mL min^{-1} (formic acid linearly changed to methanol in 20 min, then 7 min of pure methanol, and finally methanol linearly changed to formic acid water in 3 min).

Synthesis of Cu/Al_2O_3 Catalyst

Catalyst synthesis is described in detail in previous work.[30] In brief, γ-Al_2O_3 was suspended in Milli-Q water in a round bottom flask. Tetraaminecopper(II) sulfate was dissolved in dilute ammonium hydroxide solution and then added to the alumina slurry. The pH was adjusted to 9.0 with sulfuric acid and the slurry was left to stir overnight. The mixture was vacuum filtered and washed with excess Milli-Q water before drying overnight in a 323 K vacuum oven. The dried catalyst was treated in Ar at 575 K (30 min, 5 K min^{-1} heating rate) and then in H_2 at 673 K (2 h, 5 K min^{-1} heating rate). The flow was switched to Ar at 673 K (1 h) and cooled under Ar to room temperature before passivation.

Catalyst Characterization

Catalysts were characterized with a variety of techniques. A micromeritics AutoChem 2920 was used to measure pulse CO chemisorption and N_2O titration, and temperature programmed reduction (TPR) of all catalysts. Effluent gases were measured with a TCD or mass spectrometer (Cirrus 2 – Micromeritics) to quantify hydrogen, N_2O, or CO consumed and N_2 released from the catalysts. Ru and Pd dispersions were calculated using 1 (Ru or Pd) : 1 CO molecule stoichiometry. CO chemisorption was performed at 303 K. A 2:1 stoichiometric ratio of Cu sites to N_2O molecule was used for the N_2O titration over Cu/Al_2O_3, and the pulse titration was carried out at 363 K. The wt.% of Cu was measured using ICP-AES on a Vista-MPX ICP-OSE.

Reaction Kinetic Studies over Ru, Pd, and Cu Catalysts

Reactivity experiments were carried out in a 45 mL Parr batch reactor equipped with a dip tube for sampling. Cu and Ru catalysts were reduced prior to reaction at 573 K for 5 h and at 523 K for 3 h, respectively (with 3 K min^{-1} heating rates). Reductions were performed by adding the desired amount of catalyst to the batch reactor and purging with Ar to 30 bar twice and purging three times with H_2 to 30 bar. The reactor was then filled with H_2 to 30 bar and heated to the desired reduction temperature at a rate of 3 K min^{-1}. For all catalysts studied, 460 mg purified HAH was dissolved in 30 mL 2-propanol, and a desired catalyst weight (normalized between catalysts per weight of metal) was added to the Parr reactor. The reactor was purged twice with 30 bar Ar and three times with 30 bar H_2. The reactor was pressurized to 30 bar H_2 and was heated to the desired reaction temperature at a heating rate of 3 K min^{-1}. The reactor was held at temperature for the desired amount of time while samples were taken with the dip tube. H_2 was replenished after samples were taken to maintain the reaction pressure (after every 2 samples or when a 1-2 bar drop in pressure was visible). After the reaction, the reactor was cooled to room temperature by flowing air to increase cooling rates. Product samples were filtered with 0.2 µm PTFE filters and analyzed by HPLC and GC-FID after 600x or 4x dilution in IPA, respectively. ^1H, ^{13}C, and HSQC NMR were implemented for samples that contained only one or two major products for identification of molar ratios.

GC-FID analysis of hydrogenated products

A gas chromatography (GC, Shimadzu GC-2010) equipped with a flame-ionizing detector (FID) and a Zebron ZB-50 column (ZB Inferno, Phenomenex, part no. 7HG-G00411) was used to quantify PHAH=O, FHAH=O, FHAH-OH, I-HAH, and PHAH-OH. All samples were filtered with 0.2 µm PTFE syringe filters prior to injection into the GC-FID. Analytical standards PHAH=O and FHAH-OH were synthesized and used for quantification of all compounds, described in detail below.

NMR characterization of monomers

Product mixtures were collected from the Parr reactor, filtered with a 0.2 µm PTFE filters, and the solvent was evaporated. ^1H and ^{13}C nuclear magnetic resonance (NMR) spectra were obtained using a Bruker Avance-500 spectrometer. ^1H spectra were referenced to tetramethylsilane (TMS) at δ = 0 ppm and all other spectra used absolute referencing.

Reaction Kinetics Model

A reaction kinetic model was constructed to calculate reaction rate constants for each kinetic experiment condition examined. The corresponding reaction scheme (Scheme 2 or 3) was used as the network to describe hydrogenation of HAH, and a model was developed in MatLab to fit the data with the optimal reaction rate constants that best fit the data. The models incorporated a system of equations describing the hydrogenation like **Eqns. 4-7**, describing reaction over Pd and Ru in **Scheme 2**:

Eqn. 4. $r_{HAH} = -(k1 + k4 + k5)\,[HAH]$

Eqn. 5. $r_{PHAH=O} = k_1[HAH] - k_2\,[PHAH = O]$

Eqn. 6. $r_{FHAH=O} = k_2[PHAH = O] - k_3\,[FHAH = O] - k4\,[HAH]$

Eqn. 7. $r_{FHAH-OH} = k_3[FHAH = O] - \mathrm{k5}\,[HAH]$

where r_i is the rate of consumption of species *i*, [*i*] is the concentration of species *i*, and k_i is the apparent rate constant for step *i*. The model was fit to the experimental data by optimizing the rate constants using the non-linear least squares solver (lsqnonlin function) in MATLAB, and 90% confidence intervals were calculated using the nlparci function. This model provides insight into whether consecutive or parallel pathways dominate the reaction scheme over a catalyst. We note that the hydrogen pressure term is first order, and is included in the rate constants, since the hydrogen pressure was replenished throughout each reaction to account for consumption (loaded to 30 bar H_2 at room temperature). Rate constants were normalized per gram of catalyst used in each experiment.

Conclusion

We demonstrate that the reaction kinetics of HAH hydrogenation can be modelled by combined parallel and sequential lumped pathways with first order dependences of HAH and intermediate concentrations over Pd, Ru, and Cu

catalysts. We also predict optimal conditions and product yields from the lumped model and suggest conditions for further investigation of selective hydrogenation for various HAH derived products. Pd demonstrates a 4-step hydrogenation scheme that is dominated by parallel steps and yields a mixture of partially and fully hydrogenated products (FHAH=O and FHAH-OH). Ru catalysts show a 5-step hydrogenation scheme that terminates in FHAH-OH, with the Ru catalyst undergoing no pre-reduction exhibiting a larger contribution of consecutive steps dominating the hydrogenation scheme. Hydrogenation over Cu exhibits a 3-step reaction scheme and yields significant concentrations of an intermediate previously seen in small quantities over Pd and Ru catalysts. HAH hydrogenation over Cu also terminates in a different final hydrogenation product, PHAH-OH, a triol where all furan rings remained intact. Hydrogenation of furan rings was not observed over Cu. The maximum experimental yields obtained for hydrogenation intermediate products PHAH=O and FHAH=O (and derivatives) were 85% over Cu and 85% over Pd, and full conversion to FHAH-OH and PHAH-OH was possible over both Ru catalysts and the Cu catalyst, respectively. Finally, we give universal conditions for the maximum production of the various hydrogenated products for both batch and plug flow systems using the reaction kinetics parameters determined in this study.

Author Contributions

Elise B. Gilcher contributed conceptualization, data curation, formal analysis, investigation, methodology, validation, visualization, and writing; James A. Dumesic and George W. Huber contributed conceptualization, project administration, funding acquisition, supervision, and writing; Hochan Chang contributed conceptualization, resources, and writing.

Conflicts of interest

There are no conflicts of interest to declare.

Acknowledgements

The authors gratefully acknowledge the use of the NMR facilities which are funded by: Thermo Q ExactiveTM Plus by NIH 1S10 OD020022-1, Bruker Quazar APEX2 and Bruker Avance-500 by a generous gift from Paul J. and Margaret M. Bender. This material is based upon work supported by the Great Lakes Bioenergy Research Center, U.S. Department of Energy, Office of Science, Office of Biological and Environmental Research under Award Number DE-SC0018409. This work was also supported by the U.S. Department of Energy, Office of Basic Energy Sciences (DE-SC0014058).

References

1. Rosatella AA, Simeonov SP, Frade RF, Afonso CA. 5-Hydroxymethylfurfural (HMF) as a building block platform: Biological properties, synthesis and synthetic applications. *Green Chemistry.* 2011;13(4):754-793.
2. van Putten R-J, Van Der Waal JC, De Jong E, Rasrendra CB, Heeres HJ, de Vries JG. Hydroxymethylfurfural, a versatile platform chemical made from renewable resources. *Chemical reviews.* 2013;113(3):1499-1597.
3. Chang H, Bajaj I, Motagamwala AH, et al. Sustainable production of 5-hydroxymethyl furfural from glucose for process integration with high fructose corn syrup infrastructure. *Green Chemistry.* 2021;23(9):3277-88.
4. Davidson MG, Elgie S, Parsons S, Young TJ. Production of HMF, FDCA and their derived products: a review of life cycle assessment (LCA) and techno-economic analysis (TEA) studies. *Green Chemistry.* 2021;23(9):3154-71.
5. Motagamwala AH, Won W, Sener C, Alonso DM, Maravelias CT, Dumesic JA. Toward biomass-derived renewable plastics: Production of 2,5-furandicarboxylic acid from fructose. *Science Advances.* 2018;4(1):eaap9722.
6. Davis SE, Houk LR, Tamargo EC, Datye AK, Davis RJ. Oxidation of 5-hydroxymethylfurfural over supported Pt, Pd and Au catalysts. *Catalysis Today.* 2011;160(1):55-60.
7. Jae J, Zheng W, Lobo RF, Vlachos DG. Production of dimethylfuran from hydroxymethylfurfural through catalytic transfer hydrogenation with ruthenium supported on carbon. *ChemSusChem.* 2013;6(7):1158-1162.
8. Román-Leshkov Y, Barrett CJ, Liu ZY, Dumesic JA. Production of dimethylfuran for liquid fuels from biomass-derived carbohydrates. *Nature.* 2007;447(7147):982.
9. Scholz D, Aellig C, Hermans I. Catalytic transfer hydrogenation/hydrogenolysis for reductive upgrading of furfural and 5-(hydroxymethyl) furfural. *ChemSusChem.* 2014;7(1):268-275.
10. Wang G-H, Hilgert J, Richter FH, et al. Platinum–cobalt bimetallic nanoparticles in hollow carbon nanospheres for hydrogenolysis of 5-hydroxymethylfurfural. *Nature Materials.* 2014;13:293.
11. Alamillo R, Tucker M, Chia M, Pagán-Torres Y, Dumesic J. The selective hydrogenation of biomass-derived 5-hydroxymethylfurfural using heterogeneous catalysts. *Green Chemistry.* 2012;14(5):1413-1419.
12. Nakagawa Y, Tomishige K. Total hydrogenation of furan derivatives over silica-supported Ni–Pd alloy catalyst. *Catalysis Communications.* 2010;12(3):154-156.
13. Liu Y, Mellmer MA, Alonso DM, Dumesic JA. Effects of Water on the Copper-Catalyzed Conversion of Hydroxymethylfurfural in Tetrahydrofuran. *ChemSusChem.* 2015;8(23):3983-3986.
14. Jae J, Zheng W, Karim AM, Guo W, Lobo RF, Vlachos DG. The role of Ru and RuO2 in the catalytic transfer hydrogenation of 5-hydroxymethylfurfural for the production of 2, 5-dimethylfuran. *ChemCatChem.* 2014;6(3):848-856.
15. Sitthisa S, Sooknoi T, Ma Y, Balbuena PB, Resasco DE. Kinetics and mechanism of hydrogenation of furfural on Cu/SiO2 catalysts. *Journal of catalysis.* 2011;277(1):1-13.
16. Gupta K, Singh SK. Room-temperature total hydrogenation of biomass-derived furans and furan/acetone aldol adducts over a Ni–Pd alloy catalyst. *ACS Sustainable Chemistry & Engineering.* 2018;6(4):4793-4800.
17. Turkin A, Eyley S, Preegel G, Thielemans W, Makshina E, Sels BF. How Trace Impurities Can Strongly Affect the

Hydroconversion of Biobased 5-Hydroxymethylfurfural? *Acs Catalysis.* 2021;11(15):9204-9209.

18. Galkin KI, Krivodaeva EA, Romashov LV, et al. Critical influence of 5-hydroxymethylfurfural aging and decomposition on the utility of biomass conversion in organic synthesis. *Angewandte Chemie.* 2016;128(29):8478-8482.
19. Galkin KI, Ananikov VP. When Will 5-Hydroxymethylfurfural, the "Sleeping Giant" of Sustainable Chemistry, Awaken? *ChemSusChem.* 2019;12(13):2976-2982.
20. Huber GW, Chheda JN, Barrett CJ, Dumesic JA. Production of liquid alkanes by aqueous-phase processing of biomass-derived carbohydrates. *Science.* 2005;308(5727):1446-1450.
21. Barrett C, Chheda J, Huber G, Dumesic J. Single-reactor process for sequential aldol-condensation and hydrogenation of biomass-derived compounds in water. *Applied catalysis B: environmental.* 2006;66(1-2):111-118.
22. Faba L, Díaz E, Ordóñez S. Performance of bifunctional Pd/MxNyO (M= Mg, Ca; N= Zr, Al) catalysts for aldolization–hydrogenation of furfural–acetone mixtures. *Catalysis Today.* 2011;164(1):451-456.
23. Faba L, Díaz E, Ordóñez S. Hydrodeoxygenation of acetone–furfural condensation adducts over alumina-supported noble metal catalysts. *Applied Catalysis B: Environmental.* 2014;160:436-444.
24. Faba L, Díaz E, Vega A, Ordónez S. Hydrodeoxygenation of furfural-acetone condensation adducts to tridecane over platinum catalysts. *Catalysis Today.* 2016;269:132-139.
25. Strohmann M, Bordet A, Vorholt AJ, Leitner W. Tailor-made biofuel 2-butyltetrahydrofuran from the continuous flow hydrogenation and deoxygenation of furfuralacetone. *Green Chemistry.* 2019;21(23):6299-6306.
26. Silks L, Gordon J, Wu R, Hanson S. Process for preparation of furan derivatives by carbon chain extension through aldol reaction. *PCT Int Appl WO.* 2011;2011022041.
27. Olcay H, Subrahmanyam AV, Xing R, Lajoie J, Dumesic JA, Huber GW. Production of renewable petroleum refinery diesel and jet fuel feedstocks from hemicellulose sugar streams. *Energy & Environmental Science.* 2013;6(1):205-216.
28. Sutton AD, Waldie FD, Wu R, Schlaf M, Louis A, Gordon JC. The hydrodeoxygenation of bioderived furans into alkanes. *Nature chemistry.* 2013;5(5):428-432.
29. Chang H, Motagamwala AH, Huber GW, Dumesic JA. Synthesis of biomass-derived feedstocks for the polymers and fuels industries from 5-(hydroxymethyl) furfural (HMF) and acetone. *Green Chemistry.* 2019;21(20):5532-5540.
30. Chang H, Gilcher E, Huber G, Dumesic J. Synthesis of performance-advantaged polyurethanes and polyesters from biomass-derived monomers by aldol-condensation of 5-hydroxymethyl furfural and hydrogenation. *Green Chemistry.* 2021;23(12):4355-64.
31. Chang H, Bajaj I, Huber GW, Maravelias CT, Dumesic JA. Catalytic strategy for conversion of fructose to organic dyes, polymers, and liquid fuels. *Green Chemistry.* 2020;22(16):5285-5295.
32. Vannice MA, Wang S, Moon S. The effect of SMSI (strong metal-support interaction) behavior on CO adsorption and hydrogenation on Pd catalysts: I. IR spectra of adsorbed CO prior to and during reaction conditions. *Journal of Catalysis.* 1981;71(1):152-166.
33. Chen S, Wojcieszak R, Dumeignil F, Marceau E, Royer S. How Catalysts and Experimental Conditions Determine the Selective Hydroconversion of Furfural and 5-Hydroxymethylfurfural. *Chemical Reviews.* 2018;118(22):11023-11117.
34. Posada D, Buckley TR. Model selection and model averaging in phylogenetics: advantages of Akaike information criterion and Bayesian approaches over likelihood ratio tests. *Systematic biology.* 2004;53(5):793-808.
35. Hong UG, Kim JK, Lee J, et al. Hydrogenation of succinic acid to tetrahydrofuran (THF) over ruthenium–carbon composite (Ru–C) catalyst. *Applied Catalysis A: General.* 2014;469:466-471.
36. Dai C, Li Y, Ning C, Zhang W, Wang X, Zhang C. The influence of alumina phases on the performance of Pd/Al2O3 catalyst in selective hydrogenation of benzonitrile to benzylamine. *Applied Catalysis A: General.* 2017;545:97-103.
37. Zhang B, Hui S, Zhang S, Ji Y, Li W, Fang D. Effect of copper loading on texture, structure and catalytic performance of Cu/SiO2 catalyst for hydrogenation of dimethyl oxalate to ethylene glycol. *Journal of natural gas chemistry.* 2012;21(5):563-570.
38. Bradley M, Robinson J, Woodruff D. The structure and bonding of furan on Pd (111). *Surface science.* 2010;604(11-12):920-925.
39. Sitthisa S, Resasco DE. Hydrodeoxygenation of furfural over supported metal catalysts: a comparative study of Cu, Pd and Ni. *Catalysis letters.* 2011;141(6):784-791.
40. Yang J, Li N, Li G, et al. Solvent-free synthesis of C10 and C11 branched alkanes from furfural and methyl isobutyl ketone. *ChemSusChem.* 2013;6(7):1149-1152.
41. Luneau M, Lim JS, Patel DA, Sykes ECH, Friend CM, Sautet P. Guidelines to Achieving High Selectivity for the Hydrogenation of α, β-Unsaturated Aldehydes with Bimetallic and Dilute Alloy Catalysts: A Review. *Chemical Reviews.* 2020;120(23):12834-12872.
42. Biradar NS, Hengne AA, Birajdar SN, Swami R, Rode CV. Tailoring the product distribution with batch and continuous process options in catalytic hydrogenation of furfural. *Organic Process Research & Development.* 2014;18(11):1434-1442.
43. Merat N, Godawa C, Gaset A. High selective production of tetrahydrofurfuryl alcohol: Catalytic hydrogenation of furfural and furfuryl alcohol. *Journal of Chemical Technology & Biotechnology.* 1990;48(2):145-159.
44. Sexton B. A vibrational and TDS study of the adsorption of pyrrole, furan and thiophene on Cu (100): Evidence for π-bonded and inclined species. *Surface science.* 1985;163(1):99-113.
45. Shi Y, Zhu Y, Yang Y, Li Y-W, Jiao H. Exploring furfural catalytic conversion on Cu (111) from computation. *ACS Catalysis.* 2015;5(7):4020-4032.
46. Xiong K, Wan W, Chen JG. Reaction pathways of furfural, furfuryl alcohol and 2-methylfuran on Cu (111) and NiCu bimetallic surfaces. *Surface Science.* 2016;652:91-97.
47. Duarte DP, Martínez R, Hoyos LJ. Hydrodeoxygenation of 5-hydroxymethylfurfural over alumina-supported catalysts

in aqueous medium. *Industrial & Engineering Chemistry Research.* 2016;55(1):54-63.

48. Sabu SS, Simplica SJA, Tandon H, Chakraborty T. A scale of absolute hardness based on the conjoint action of other properties. *Molecular Physics.* 2021:e1992521.